Sebastian Stark[1]
Institute of Solid Mechanics,
Technische Universität Dresden,
01062 Dresden, Germany
e-mail: Sebastian.Stark1@tu-dresden.de

Matthew R. Begley
Department of Mechanical Engineering,
University of California,
Santa Barbara, CA 93106
e-mail: begley@engr.ucsb.edu

Robert M. McMeeking
Department of Mechanical Engineering,
University of California,
Santa Barbara, CA 93106;
Materials Department,
University of California,
Santa Barbara, CA 93106;
INM-Leibniz Institute for New Materials,
Campus D2 2,
66123 Saarbrücken, Germany;
School of Engineering,
University of Aberdeen,
King's College,
Aberdeen AB24 3UE, UK
e-mail: rmcm@engineering.ucsb.edu

The Buckling and Postbuckling of Fibrils Adhering to a Rigid Surface

Recent experiments in which arrays of compliant fibrils are compressed axially against a rigid surface and then released have shown that there is load-displacement hysteresis during this process, accompanied by buckling and unbuckling of the fibrils. Furthermore, the adhesive performance of the system is decreased by such prior buckling. We present a model describing the buckling and postbuckling characteristics of a fibril with an aspect ratio of 10 or greater. The possibility during buckling of partial detachment of the end of the fibril is taken into account. The results are presented and discussed for both load and displacement control and the load-displacement hysteresis is identified. It is found that due to instabilities sudden spreading and shrinkage of the adhered area at the end of the fibril can accompany the hysteresis. Numerical results are provided to substantiate the findings and possible reasons for the observed influence of buckling on adhesive performance are reviewed. [DOI: 10.1115/1.4023107]

1 Introduction

Many animals use adhesive contact to stick to rough or smooth surfaces. Most of them, like geckos, spiders or flies, have developed fibrillar structures. According to the "contact splitting principle," these structures allow for a better adhesive performance with decreasing fibril radii [1]. Based on this finding, there are current efforts to develop artificial dry adhesives based on fibrillar structures (e.g., see Ref. [2]).

Another important factor, besides the resistance of the adhesive bond against pull-off, is the adaptability of adhesive systems to rough surfaces. Ideally, the adhesive material would deform plastically to establish a good contact over the whole surface. However, an aim is that the process of attachment and detachment should be repeated for a high number of cycles without any decay in adhesive performance. Hence, plasticity is to be avoided and the adaptability of compliant fibrillar systems is an advantage. In this regard, buckling of fibrils is an asset for adaptive contact. When the critical buckling load of a fibril is exceeded, large compressive strains are possible without significant increase in the applied load. Thus, an array of microscopic fibrils can behave on the macroscopic scale as a nonlinear elastic system having properties similar to a plastic material in that extensive crushing is possible without significant elevation in stress. In contrast to plasticity, unloading of a buckled, elastic, fibrillar system is reversible and, in principle, permits re-use for adhesion without damage. These considerations are predicated on the ability of the fibril to retain its adhesion after it has buckled, and to recover an unbuckled shape without damage upon being unloaded. In contrast, recent results suggest that buckling of fibrils leads to a reduction of adhesion when the system is separated thereafter [3]. In addition, experimental results indicate that while the unbuckled shape of a fibril is recoverable upon unloading, there is load-displacement hysteresis in the process [4,5]. It has been observed that unbuckling takes place at a different load than buckling. This is attributable to the fact that the ends of the fibrils detach from the compressing surface and lose adhesion to it during buckling and postbuckling. This phenomenon changes the boundary conditions on the end of the fibril and consequently modifies the load at which the fibril will unbuckle. Hui et al. [4] developed a theoretical model for this process based on Euler–Bernoulli beam theory and linear elastic fracture mechanics, which allows the determination of the buckling and unbuckling loads dependent on the extent of detachment. We now extend this approach in order to predict load-displacement curves during buckling and unbuckling of a fibril. The resulting load-displacement curves give considerable insight into the buckling, postbuckling and unbuckling behavior of fibrils. Furthermore, the results suggest that effects of viscosity, inertia and friction may play an important role in the buckling and adhesion characteristics of fibrillar mats.

As noted above, Glassmaker et al. [3] reported that buckling can be detrimental to fibrillar adhesion. Using a glass sphere, they indented arrays of Polydimethylsiloxane(PDMS)-fibrils having a rectangular cross-section with one dimension much greater than the other one and then detached the probe from the fibrils. When buckling of fibrils occurred, a decrease by up to a factor of 4 in the effective work of adhesion and, thus, the pull-off force during the detachment segment of the load cycle was observed. Such a result is surprising, because one would expect that fibrils that detach during buckling under compression would reattach when the probe is being separated from the fibrils and they are able to unbuckle. Apparently they do not, and possible reasons for this phenomenon will be reviewed in the discussion of our results.

It is emphasized that this paper addresses the buckling behavior of artificial fibrillar adhesives. Natural adhesive systems are far more complex and we acknowledge that these may not be described with the results given here. However, an exact reproduction of the structures found in nature seems to be illusive to date, due to the limitations of current manufacturing methods. Therefore, strong simplifications of these natural structures are

[1]Corresponding author.

Manuscript received January 31, 2012; final manuscript received November 8, 2012; accepted manuscript posted November 28, 2012; published online May 23, 2013. Assoc. Editor: Lawrence A. Bergman.

necessary. This has led to the development of adhesive surfaces being covered with straight fibrils. We believe that our considerations are relevant for the understanding and further development of these quite simple fibrillar surfaces. The physics of natural adhesive devices of animals like geckos are discussed in detail, for example, in the comprehensive works of Gao et al. [6], Gao and Yao [7], and Yao and Gao [8]. The results given therein suggest that many more concepts, like anisotropy of the fibrils material, asymmetric fibrils, inclined fibrils, size reduction of the fibril cross section and hierarchical structures, can strongly improve the adhesive performance. However, consideration of these aspects is beyond the scope of this paper.

2 Model of Buckling

Our model describes the behavior of a single fibril compressed by a platen as shown in Fig. 1. The fibril tip at its upper end is partially adhered to the platen, which is a rigid, smooth surface. For simplicity, the fibril has a rectangular cross-section and the platen is allowed to move freely in the lateral direction while its rotation is prohibited. On the other fibril end, the lower one in the figure, the boundary condition is taken to be fully clamped with no lateral motion or rotation. Nevertheless, all formulae in the analysis (see Appendix A) are developed in terms of "shape functions," which represent the given boundary conditions. Thus, the end conditions can be easily adjusted by using appropriate shape functions. For example, the lateral displacement at the adhered end of the fibril, the upper end in the figure, may be eliminated if so desired. As a consequence, conditions that are common in experiments with a fibrillar bed probed by an indenter may be readily duplicated. Here, the laterally free boundary condition at the fibril tip is chosen for reasons of simplicity. Furthermore, photographs of the buckling process [4,9] indicate that the fibrils in the experiments buckle like expected for the laterally free boundary condition (we suspect that this is due to the experimental setup or the compliance of the backing layer on which the fibrils are patterned). Additionally, it is noted that the results obtained for the laterally constrained case are qualitatively similar.

The undeformed length of the fibril is l_0 and l denotes the distance between the tips of the fibril in the deformed configuration. This directly yields the relative axial displacement $u = l_0 - l$ between the fibril ends, which is also the displacement of the platen. This parameter is taken to be positive when the platen is moved downwards to place the fibril in compression. We define a positive applied load, F, to be one that applies compression to the fibril. Fibril deflections in the lateral direction are identified as $w(z)$, where z is the axial coordinate parallel to the undeformed fibril. The fibril tip adjacent to the platen is partially attached, and partially detached, and the detachment is assumed to be a rectangle of length a across the fibril and all the way through the fibril thickness. The width of the fibril is b and its thickness is h. The product E^*I is the bending stiffness of the fibril, where E^* is the generalized elastic modulus, equal to the Young's modulus E of the material in plane stress and $E/(1-\nu^2)$ in plane strain, where ν is Poisson's ratio.

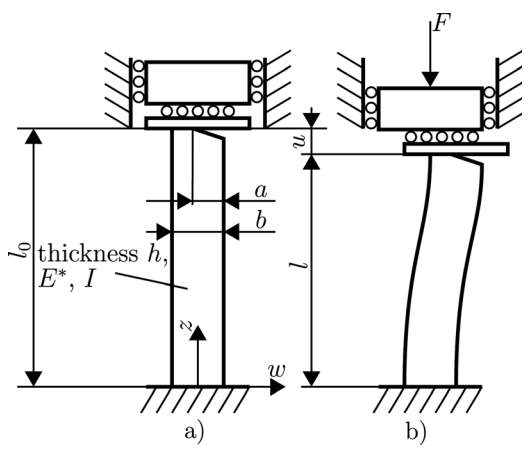

Fig. 1 Model for buckling of the fibril: (*a*) undeformed configuration; (*b*) deformed configuration

In our model, the bending behavior of the fibril is approximated as that of an Euler–Bernoulli beam. This limits the aspect ratio, l_0/b, which can be analyzed to approximately $l_0/b \geq 10$. Furthermore, we use d^2w/dz^2 as the curvature of the fibril, so that the rotation, dw/dz, has to stay small enough for this approximation to remain valid.

The adhering ligament on the tip of the fibril is allowed to detach, with such a detachment seen as an interface crack. The adhesive behavior is assumed to be completely reversible. Thus, the work of adhesion is the same during detachment and attachment. Nevertheless, the approach can be easily extended to cases involving adhesion hysteresis as discussed below. It is assumed that the tangential tractions on the adhering ligament vanish. This corresponds to a no friction boundary condition, a somewhat unrealistic assumption. However, we believe that the general behavior of the fibril is not strongly influenced by the neglect of friction. The results of Spuskanyuk et al. [10] indicate that the effect of friction is only pronounced for relatively short detachments, probably attributed to the corner singularity. Note that we do not imply that friction is unimportant during detachment of the fibril tip in tension, where large distortions can introduce significant frictional shear stresses that influence pull-off. We concern ourselves with partial detachment of the fibril tip during compression and fibril buckling, where we believe the influence of friction on the processes involved is less important. Furthermore, we assume that any zone of inelastic material behavior in the fibril is small compared to a and $b-a$, so that linear elastic fracture mechanics can be utilized. Moreover, the surface adjacent to the adhering tip is modeled as a rigid surface. Thus, complications associated with the presence of an interface crack between two differing elastic materials are avoided. Given these assumptions, standard fracture mechanics solutions for a crack in an isotropic linear elastic material can be used to determine the stress intensity factor (see Appendix A). The detachment is modeled as one side of such a crack. The mode I stress intensity factor, K, is utilized to characterize the detachment driving force. In contrast to the use of the (always positive) energy release rate G, this allows for the exclusion of physically meaningless solutions with an overclosure of the detachment, i.e., those with a negative K. The relationship between the stress intensity factor and the energy release rate is

$$G = \frac{K^2}{2E^*} \tag{1}$$

the relationship relevant to an interface crack (and thus, an adhesion) between a rigid and a compliant surface, where frictional shear stresses are neglected. The factor 2 in the denominator takes into account the fact that only one surface of the crack deforms.

The influence of the detachment on the elasticity of the system is taken into account by including additional compliance at the fibril tip, i.e., springs are introduced at the fibril tip connecting it to the platen, with stiffness calibrated to the extent of the detachment (see Appendix A). This approach was previously used by Hui et al. [4] to calculate the buckling loads of fibrils dependent on the detachment length. The influence of shear compliance associated with the presence of a detachment will be neglected here, consistent with our use of Euler–Bernoulli beam theory.

For a given load, F, the unknowns in the solution are detachment length a and axial displacement u. Under displacement control, u is specified and we have to determine F. This requires two equations: the first represents the "detachment equilibrium," which incorporates the requirement that the energy release rate G of the system has to be equal to the work of adhesion W_{ad} for all admissible states, other than those for which $a = 0$ and $a = b$ and the second equation is derived from the law of conservation of

mass, used to ensure that the buckled length of the fibril is consistent with its undeformed length [11].

3 Results

Details of the analysis can be found in the Appendix A. For clarity, we present here only the main results. For this purpose, the following normalized quantities are defined:

$$\kappa_0^2 = \frac{F l_0^2}{E^* I}$$
$$\bar{K} = \frac{K}{E^* \sqrt{b}} \qquad (2)$$
$$\bar{K}_{\mathrm{ad}} = \sqrt{\frac{2W_{\mathrm{ad}}}{bE^*}}$$
$$\bar{a} = \frac{a}{b}$$

Since the resulting equations are nonlinear, the solution is obtained numerically. The results for an aspect ratio of $l_0/b = 10$ are shown in Fig. 2 as normalized load κ_0^2 versus normalized axial displacement u/l_0. Each result depicted in Fig. 2 involves an unbuckled or buckled configuration, having a detachment at the fibril end where it touches the platen. The load and displacement are consistent with each other through the requirement that the deformed length of the fibril, possibly in a buckled state, is consistent with the undeformed length in terms of the axial stress and strain it suffers (i.e., conservation of mass). The load and fibril configuration, including the detachment length, combine to determine the stress intensity factor experienced at the detachment front. Lines of equal normalized stress intensity factor $\bar{K} = \bar{K}_{\mathrm{ad}}$ are drawn as continuous lines for detachments which are associated with a stable detachment equilibrium under displacement control, while a dotted line indicates an unstable detachment equilibrium. In the latter case, the detachment must extend or contract but cannot remain as it is. These lines indicate the paths that a given fibril will follow, or try to follow, during buckling or unbuckling at a given work of adhesion. The linear elastic line corresponding to the absence of buckling and limiting buckling loads are drawn as thick lines. The upper almost horizontal limit corresponds to the case of a fully attached fibril ($\bar{a} = 0$) buckling without detaching from the platen and without it rotating, while the lower almost horizontal limit represents a boundary condition in which the fibril tip is free to rotate without resistance. Note that these curves have a slightly positive slope. This is caused by the reduction of the distance between the ends of the fibril in compression, which in turn increases the buckling load. The dashed lines, drawn with alternating dots and dashes, are associated with detachments of constant size (i.e., equal values of $\bar{a}$). These lines represent the paths followed by the system when the fibril buckles, but the detachment is able to neither lengthen or shorten. It is straightforward to identify the stability of the detachment equilibrium based on these curves. If we take, e.g., point B in Fig. 2 and increase (decrease) the detachment length by going vertically downward (upward) at a constant displacement u/l_0, the normalized stress intensity $\bar{K}$ increases (decreases), which means that the detachment equilibrium is unstable if displacement control is applied and the work of adhesion is constant on the whole adhering surface. Consequently, the detachment needs to grow (shrink) dynamically. We do not resolve this dynamic behavior in our considerations. Rather, it is assumed that the state of the system is always associated with a stable detachment equilibrium. Therefore, once an unstable detachment equilibrium is detected, the system experiences a sudden jump to a state being associated with a stable detachment equilibrium. Note that such a treatment of the problem is only possible if the stable detachment equilibrium is unique. In the following, we refer to the transition between an unstable and a stable detachment equilibrium with "dynamic detachment/reattachment."

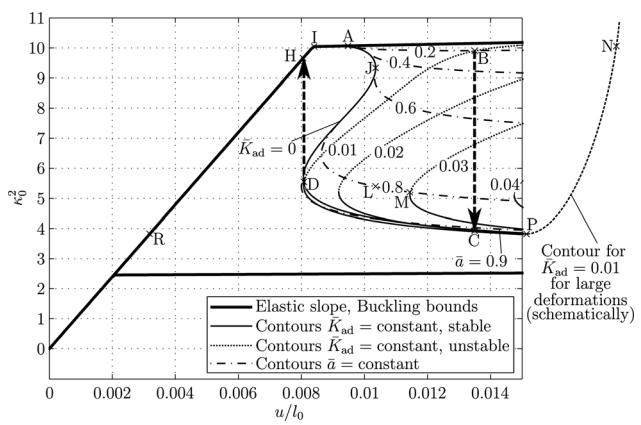

Fig. 2 Load-displacement curves for an aspect ratio of 10

It is notable that in the vicinity of point D in Fig. 2 some contours of constant $\bar{K} = \bar{K}_{\mathrm{ad}}$ intersect each other (e.g., the contours $\bar{K}_{\mathrm{ad}} = 0$ and $\bar{K}_{\mathrm{ad}} = 0.01$). The same holds true for lines of constant detachment length (not visible in this plot). This implies that the solutions in this region are not uniquely characterized by the displacement u/l_0 and the normalized force κ_0^2, i.e., configurations with different adhesion energies and detachment lengths may lead to the same combination of end point displacement and applied load. Consequently, one has to take the adhesion energy and detachment length into account to distinguish between such cases. Furthermore, in this area of the figure, it is no longer easily possible to examine the stability of the detachment equilibrium graphically. Instead, it is advantageous to calculate the change in detachment driving force for a small change in detachment length, i.e., if the detachment driving force increases (decreases) for an infinitesimal increase (decrease) in detachment length, the state is unstable (see also Appendix A).

Great care was taken to represent the correct asymptotic behavior for the detachment-related fibril tip compliances for long detachment lengths. Nevertheless, we cannot exclude the possibility that the phenomenon of intersecting contours for equal stress intensity factor and equal detachment length is caused by inaccurate curve fits in results used to obtain the fibril tip compliances or other numerical errors due to the singular nature of the fibril tip compliances for $\bar{a} \to 1$.

3.1 Fibril Behavior Under Displacement Control. To discuss the general behavior during a load cycle under displacement control, we assume an initial detachment of normalized length $\bar{a}_{\mathrm{init}} = 0.2$. Such a flaw could be caused by a radius at the edge of the fibril, though it is larger than seems likely from such a source. The critical normalized stress intensity factor $\bar{K}_{\mathrm{ad}}$ is taken to be zero on the initially detached surface and $\bar{K}_{\mathrm{ad}} = 0.01$ on the initially adhered surface. The latter value corresponds to a work of adhesion equal to 0.05 J/m^2 for a 500 micron wide fibril of PDMS having a generalized Young's modulus of $E^* = 2$ MPa. Note that typical fibril dimensions are much smaller. However, fibrils with a width on the order of 10 microns and an aspect ratio of 10 would detach at very large deformations, which cannot be predicted accurately with the presented theory. Thus, the results can be interpreted quantitatively only for materials which are at least one order of magnitude stiffer than PDMS, when realistic geometries are considered. The same restriction is imposed by the use of linear elastic fracture mechanics since for small and compliant fibrils of PDMS the cohesive (adhesive) zone can reach the order of the fibril width. Nevertheless, finite element simulations indicated the same qualitative behavior as described here also for fibril properties which are typically used in experiments, e.g., a fibril width of 20 microns and an aspect ratio of 3.

The path in Fig. 2 followed by the fibril starts at the origin where there is no applied load, and then compression is applied as

the platen moves downwards until the fibril buckles. Prior to buckling, the path followed is thus, the linear elastic line from the origin to the point I, where buckling, i.e., instability of the fundamental equilibrium path occurs. It is assumed that the initial detachment has no influence on buckling when the fibril is first compressed. This is equivalent to allowing the detached fibril surface on its tip to make contact with the platen in compression even though they are not adhered. Instability, therefore, first occurs when the load reaches the critical value for buckling associated with a fibril end that is fully constrained against rotation, i.e., the upper buckling limit shown in Fig. 2. As a consequence, the path in Fig. 2 followed by the fibril after buckling consists of the upper buckling limit that is almost horizontal and passes through the point A in Fig. 2. As the path is traversed from I to A, the distance between the fibril ends is reduced, which leads to an increase of the buckling amplitude. However, the axial load barely increases during this postbuckling behavior.

We assume that buckling takes place in the direction, which tends to open the detachment and cause the nonadhered surface of the fibril tip to move away from the platen. At first this leads to a decrease of the compressive tractions on the detachment surface, and the postbuckling behavior at first occurs with the fibril tip still constrained against rotation. This causes the path in Fig. 2 followed by the fibril to move from the buckling point at I in Fig. 2 towards the point marked A, as previously noted. At or near point A in Fig. 2 the tractions on the detached segment of the tip of the fibril fall to zero and the detached segment is finally able to separate itself from the platen. As a consequence, the detachment unzips with increasing axial displacement until it is entirely open. Thereafter, the load-deflection curve for the fibril under displacement control follows the line for constant detachment length $\bar{a} = 0.2$ from point A in Fig. 2 to point B so that the axial displacement of the fibril tip and hence, the buckling amplitude is increased further. As the path from A to B in Fig. 2 is followed, the stress intensity factor increases, and hence the energy release rate at the detachment front increases as well.

At point B in Fig. 2 the detachment tip energy release rate becomes equal to the work of adhesion, and therefore the detached length is capable of growing. As previously discussed, the detachment equilibrium at this point is unstable in displacement control. But now, shrinking of the detachment is prohibited because the work of adhesion is assumed to be zero for detachments shorter than $\bar{a} = 0.2$. Consequently, the detachment rapidly grows until the fibril is almost completely detached from the platen. Since the system is under displacement control, the load falls dramatically while the detachment is extending, and the system follows the path from B to C in Fig. 2. Note that at point C in Fig. 2, the detachment is approximately 95% of the way across the fibril tip. At point C the energy release rate is once more equal to the work of adhesion, and extension of the detachment is arrested. Note again, that we neglect the role of inertia and dissipation in this process; we further comment on this in Sec. 4. After the point C is reached the state is stable once more and we can move the platen downwards to increase the axial fibril displacement to further compress the fibril and increase the buckling amplitude. This will cause the system to follow the line for $\bar{K}_{ad} = 0.01$ to the right of point C in Fig. 2, with the load falling slightly as the buckling amplitude and the detachment length both increase. Note that the relevant line is not visible in Fig. 2 as the lines for constant $\bar{K} = \bar{K}_{ad}$ converge in this region of the diagram. Note also, that the predictions of the model will become invalid at a certain point because of excessive deformations leading to a violation of the infinitesimal strain assumptions involved in the presented model. In addition, the fact that we require the rotation of the fibril to remain modest limits the extent of validity of our solution. Furthermore, the fibril will eventually be compacted under extreme crushing by the platen, causing the axial force to increase again as indicated by the dashed line for $\bar{K}_{ad} = 0.01$, which is drawn schematically to the right of the diagram in Fig. 2. The associated increase in system stiffness and compressive load can be seen clearly in the experimental results of Hui et al. [4]. It is unclear when this phenomenon takes over relative to the buckling and postbuckling events summarized in Fig. 2.

If, instead, at point C in Fig. 2 the platen is raised and the fibril tip displacement is decreased, the system follows the curve in Fig. 2 corresponding to $\bar{K}_{ad} = 0.01$, from points C to D. It does so because the path from C to D with $\bar{K}_{ad} = 0.01$ involves stable configurations of the detachment, meaning that an increase in detachment length when the fibril tip is held stationary leads to reductions in the stress intensity factor and detachment tip energy release rate. Note that the process of following the path in Fig. 2 from points C to D involves a slight reduction in length of the detached segment of the fibril tip, due to the detachment readhering to the platen. This process continues until the point D in Fig. 2 is reached. Above point D in Fig. 2, there are no solutions other than the linear elastic line for an unbuckled fibril. Therefore, under displacement control, the system has no option other than to unbuckle with the detachment zipping shut in a dynamic process so that the fibril tip readheres again completely, or almost completely, to the platen. As a consequence, the system now follows a path in Fig. 2 from point D to point H. Further raising of the platen once point H is reached causes a decrease in the axial displacement of the fibril tip, leading to elastic unloading from point H in Fig. 2 towards the origin. Note that we have demonstrated that load-displacement hysteresis exists for adhesive fibrillar systems compressed beyond buckling and then released, with the hysteresis loop under displacement control consisting of the cycle from H to I to A to B to C to D to H.

The description of the process of applying compressive loading to buckle a fibril and the removal of the load, with displacement control utilized, can be repeated for various values of $\bar{a}_{init}$ and $\bar{K}_{ad}$, with detail differences in the behavior revealed. For example, in cases where the detachment length is greater than $\bar{a}_{init} \approx 0.5$, an additional instability can occur in displacement control at the point marked J in Fig. 2 due to the involute in the curve representing the path for a fixed value of $\bar{a}$. In the case of a system with $\bar{a}_{init} = 0.8$ and $\bar{K}_{ad} = 0.03$, the resulting load jump will take the system from the point J to the point marked L on the lower branch of the curve for $\bar{a} = 0.8$. As above, this involves a reduction in the applied load and an increase in the buckling amplitude. Further compression of the fibril will induce the system to travel along the line for constant $\bar{a} = 0.8$ until the point M in Fig. 2 is reached, where the detachment tip energy release rate is equal to the work of adhesion. Further compression of the fibril will cause the detachment on its tip to extend, but in this case the detachment equilibrium is stable and the system will follow a path in Fig. 2 given by the line for a constant $\bar{K}_{ad} = 0.03$, such that the applied load gradually diminishes. Reversal of the direction of motion of the platen, i.e., it is now raised in the configuration depicted in Fig. 1, allows the detachment on the fibril tip to reduce in length with the system retracing its path along the line of constant $\bar{K}_{ad} = 0.03$. When the point M in Fig. 2 is reached once more, what happens next depends on whether the system is limited to a detachment no smaller than $\bar{a} = 0.8$. If this is the case, then as the tip axial displacement is reduced, the system will stably follow the path in Fig. 2 associated with a detachment of length $\bar{a} = 0.8$, with the load gradually increasing. This will continue until the point in Fig. 2 equivalent to D is reached. Then, the system jumps on a path in Fig. 2 vertically upwards, a response analogous to that involved in the jump the previous system experiences in going from points D to H in Fig. 2. If a detachment of length less than $\bar{a} = 0.8$ is permitted, the detachment equilibrium of the system with $\bar{a}_{init} = 0.8$ initially and $\bar{K}_{ad} = 0.03$ again becomes unstable when it returns to the point M in Fig. 2 having been compressed beyond the level associated with that point. As a result of this instability, the system experiences a jump involving a path that takes it vertically upwards in Fig. 2 from the point M until the upper buckling line is reached, in which case the fibril tip is (almost) completely reattached to the platen, with either a very small or no detachment remaining. Obviously the applied load has

jumped up to a level slightly above the initial critical value for buckling. Thereafter, as the platen is further raised and the fibril tip axial displacement is reduced, the buckling amplitude steadily diminishes and the applied load reduces slightly, until the point I in Fig. 2 is reached, at which stage unbuckling occurs. The example just given illustrates the fact that dynamic detachment closure during unloading does not necessarily bring the system back to a point on the elastic loading line for unbuckled fibrils, i.e., not to a point like H in Fig. 2. In the case of $\bar{K}_{ad} = 0.02$ the system will jump to a point in Fig. 2 on the upper buckling limit line adjacent to the point A.

Furthermore, it is also possible to construct the load-displacement hysteresis for a fibril experiencing irreversible adhesive behavior, i.e., adhesion hysteresis. In the extreme case, it can be assumed that the detachment extends with a value of $\bar{K}_{ad} > 0$, but diminishes in length with $\bar{K}_{ad} = 0$. For the example above, in which $\bar{a}_{init} = 0.2$ and $\bar{K}_{ad}$ for extension of the detachment is 0.01, the system follows the same path in Fig. 2 as before until the point C is reached. Thereafter, it follows a line in Fig. 2 of constant detachment length from point C towards the point D after the loading direction is reversed until the curve corresponding to $\bar{K}_{ad} = 0$ is reached. Subsequently, the system proceeds on this curve in Fig. 2 until the point at which it becomes vertical, just above point D in Fig. 2. From here, under displacement control, there are no solutions involving a buckled configuration if the axial displacement of the end of the fibril is to be reduced, i.e., the platen in Fig. 1 is to be moved upwards. Therefore, the fibril must unbuckle and dynamic closure of the detachment occurs. We note that, in this case, adhesion hysteresis has made almost no difference to the loading and unloading behavior of the system, and the load-displacement response is almost identical with and without adhesion hysteresis.

3.2 Fibril Behavior Under Load Control. Under load control the load-displacement curves can be constructed in an analogous way. Consider again the case where $\bar{a}_{init} = 0.2$ and $\bar{K}_{ad} = 0.01$. This system will still follow a path from the origin to the point I when the fibril is first compressed, and will buckle at point I. After buckling, the axial displacement will increase significantly while the buckling amplitude grows larger, and the system will follow the path in Fig. 2 from I to A. The applied load rises slightly during this postbuckling phase from points I to A, so the process remains stable. However, in the vicinity of A, the detachment on the fibril will begin to separate from the platen, but the stress intensity factor at this stage is zero. From A onwards, all relevant, feasible equilibrium locations having $\bar{K}_{ad} = 0$ and $0 < \bar{a} \leq 0.2$ or $0 < \bar{K}_{ad} \leq 0.01$ and $\bar{a} = 0.2$ or $\bar{K}_{ad} = 0.01$ and $\bar{a} > 0.2$ are associated with a load smaller than that applied at the point A in Fig. 2. For the system to reach these equilibrium locations, the applied force would have to be reduced, forbidden under load control. Therefore, at constant applied load, the system will experience a sudden, dynamic axial displacement jump to further compress the fibril, while its buckling amplitude also increases dramatically. This process involves a path in Fig. 2 that takes the system horizontally from point A rightwards out of the range depicted in the diagram. Given the assumptions of our model, including infinitesimal strain and the validity of Euler–Bernoulli beam theory, there is no satisfactory solution in force control that will terminate the associated dynamic response of the fibril. Instead, compaction of the fibril will occur, resulting in a crushed fibril that supports the load being applied by the platen. The corresponding point is labeled N on the schematically drawn continuation of the contour $\bar{K}_{ad} = 0.01$ for large deformations on the right of the graph in Fig. 2.

Further increase of the applied load will encounter a very stiff response of the system, since the fibril is now fully compacted and deforms in a manner akin to a solid layer of material. If the load is now decreased, reducing the compression being applied to the compacted fibril, a path as indicated by the dashed line to the right of the diagram in Fig. 2 will be followed. It is assumed that the equilibrium states on this line are stable. Note also that we exclude for this discussion any additional adhesion between the side-faces of the fibril and the platen as well as sticking due to self contact of the fibril. The path schematically drawn as the dashed line downwards from N in Fig. 2 will be followed while the compaction of the fibril is decreased during decrease of the applied load. At the minimum of this path, at point P in Fig. 2, the only possible solution for further decrease of the applied load can be found on the line corresponding to axial compression of the unbuckled fibril, i.e., the line from the origin to I. Thus, the fibril has no option other than to straighten up immediately to the point marked R in Fig. 2. This process is accompanied by a significant axial displacement jump of the fibril tip that involves the platen moving upwards in the configuration depicted in Fig. 1. Further reduction of load then allows the system to follow a path in Fig. 2 that takes it back to the origin, at which stage it is, of course, free of applied load and it has returned to its original length.

The same approach as we have just described can be used to trace out the loading and unloading behavior of a compressed fibril under load control subject to different values of the initial detachment length and work of adhesion, where, of course, the details of what happens and the exact load-displacement hysteresis will vary from case to case. The characteristics of the behavior of the system under load control for these other cases will be quite similar to the events we have just described. Specifically, after the surfaces involved in the initial detachment separate at or near point A in Fig. 2, the situation is almost always unstable, and the amplitude of buckling together with the axial displacement of the fibril tip increase dramatically. Only for very small initial detachments and a high work of adhesion is a small stable increase of the applied load likely after opening of the initial detachment.

It should be noted here that the described compaction behavior during subsequent dynamic collapse involves a violation of most of the assumptions built into our model, and a more realistic treatment may require the relaxation of the restriction to infinitesimal strains, the use of something other than Euler–Bernoulli beam theory, the inclusion of the effects introduced by transverse shear stress in the behavior of the fibril, and the possibility of contact.

Note that for aspect ratios greater than 10 the appearance of the diagram equivalent to Fig. 2 will change little, with the upper and lower buckling limits, representing the cases of buckling with the fibril tip fully constrained against rotation and able to rotate freely without constraint, remaining approximately in the same location in the resulting figure. Furthermore, the lines representing the equilibrium states in the buckled configuration associated with a given initial detachment length and a given value of $\bar{K}_{ad}$ will have a similar appearance to those in Fig. 2 even when the aspect ratio of the fibril is longer than 10. The only major change is that the slope of the linear elastic loading and unloading line from the origin to the buckling point will be different, dependent on the fibril aspect ratio. Therefore, there is little difference in the behavior of the system for higher aspect ratios of the fibril compared to that which we have already described. However, the physical result is that the buckling all happens at smaller axial compressions when the aspect ratio of the fibril is greater than 10, with the buckling loads scaling in proportion to b^2/l_0^2.

3.3 Numerical Results. Figure 3 shows a finite element result for the displacement controlled load cycle described above in which $\bar{K}_{ad} = 0.01$ and $\bar{a}_{init} = 0.2$. The finite element results are plotted along with the Euler–Bernoulli beam theory solution. The numerical procedure is presented in detail in Appendix B. The numerical and Euler–Bernoulli beam theory results for this example are found to be virtually identical. Furthermore, the finite element analysis successfully predicts the dynamic detachment of the fibril tip from the platen, i.e., the precipitous drop in the load at the right hand end of the graph. On the other hand, the finite element analysis no longer converges after a small amount of dynamic

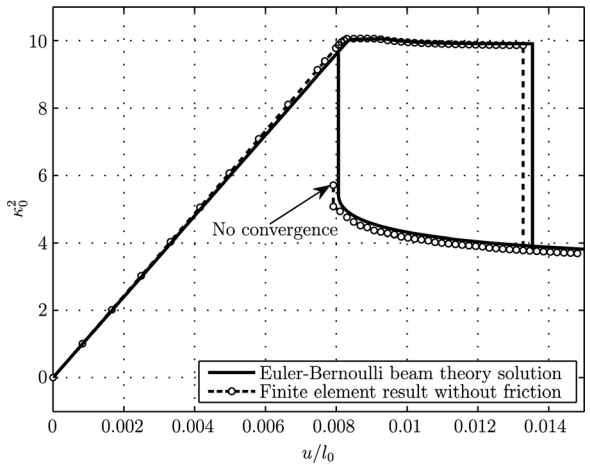

Fig. 3 Finite element result in comparison with the Euler–Bernoulli beam theory solution for aspect ratio 10, $\bar{K}_{ad} = 0.01$, $\bar{a}_{init} = 0.2$

reattachment of the fibril tip to the platen has occurred, i.e., at the location marked "No convergence" in Fig. 3. This is due to shortcomings of the solution procedure, which cannot treat the sudden reattachment of the fibril tip properly. Note the excellent accuracy of the Euler–Bernoulli beam theory solution compared to the finite element results. Given the idealizations involved in beam theory, we suspect that some error compensation is involved in the outcome.

4 Discussion

Euler–Bernoulli beam theory and finite element method results were presented describing the behavior of an adhering fibril in compression. Due to the increasing compressive load, the fibril buckles, leading to the detachment of the initially attached surface on its tip. Reattachment takes place upon unloading of the fibril when it unbuckles. Both events are found to be dynamic processes given the boundary conditions, leading to a significant hysteresis in the load-displacement curve. The prediction of jumps in the applied force or the displacement is consistent with experimental results [4,5]. We note that our model is restricted to cases where fibrils have an aspect ratio of around 10 or greater, a condition that is not met in most experiments on fibrils adhered to substrates, as this ratio is usually no more than 3 in the experiments [4,5]. The restriction to an aspect ratio of 10 or greater ensures the validity of Euler–Bernoulli beam theory. Moreover, we assume plane strain behavior of the fibril in the Euler–Bernoulli beam theory analysis, mainly to simplify the geometry of the detached surface on the fibril tip. In contrast, the fibrils used in the experiments usually have a cross-section that invalidates our plane strain assumption, except the results of Sharp et al. [5] with platelike fibrils, having a rectangular cross-section with one dimension much greater than the other one. Nevertheless, we believe that the phenomena we identify in the behavior of such long, plane strain, adhering fibrils under compression is relevant to the response of the stalkier rectangular or cylindrical fibrils that are used in the experiments. This conjecture was also supported by further finite element simulations. However, discussion of these simulations is beyond the scope of the paper due to the difficulties arising from excessive deformations, contact of the side faces of the fibril with the platen and self-contact of the fibril.

In the experiments, a PDMS surface, patterned with stalky fibrils, is brought into contact with a smooth, stiff probe so that the tips of the fibrils adhere to it. After contact is made, the tip of an adhering fibril is nominally fully attached to the probe surface, without a detached segment. However, fibrils generally have an edge radius around the circumference of the tip, acting as a very small detachment at the perimeter of the adhesion between the fibril and the probe surface. When such a fibril buckles under compressive load, it will behave as we have described above, but following the path of response relevant to the case having a very small initial detachment. We now describe the response of such a fibril in both displacement and in load control to suggest what is happening in the experiments when the fibrils of a patterned surface simultaneously buckle and unbuckle. Note that we describe the behavior that we believe occurs between a set of fibrils patterned onto a flat surface when it is compressed against a flat probe. Often the probe is spherical, introducing further complications in the processes of fibril attachment, buckling, unbuckling and detachment. However, we neglect such complications at present and concentrate on phenomena we believe arise in the case of fibrils on a flat surface adhering to a stiff, flat probe.

In the case of displacement control, the response of fibrils with a very small detachment will be quite analogous to the behavior for displacement control described above. That is, buckling will occur at the point I marked in Fig. 2, and as the distance between the tips of the fibrils and their bases is reduced during postbuckling behavior, the load will rise slightly as the path towards A in Fig. 2 is followed. Thereafter, the detached segment separates, which may lead to a decrease in the applied force. In the next step, the energy release rate at the detachment front increases. However, during this stage of postbuckling, due to the very small size of the pre-existing detachment, the load will remain very close to the level indicated by the upper thick, almost horizontal line to the right of A in Fig. 2 that gives the post buckling behavior of a fibril whose tip is completely attached to the platen. This behavior will persist to a relatively large displacement of the tip of the fibril, continuing until the energy release rate rises to the critical level that permits the detachment to grow. Prior to this happening, large deformation and rotation of the fibril may induce contact of the fibril with the surface at its base, leading to crushing effects and a rise in the necessary applied load. Let us assume that such effects are absent. In that case, when critical growth of the detachment commences, it will dynamically extend until the fibril tip is almost completely detached from the probe, and the load will fall to a level quite close to that indicated by the thick, almost horizontal line in Fig. 2 that signifies the buckling load of a fibril whose tip is free to rotate when buckling first occurs. If the fibril is further compressed, the applied load will remain at this level until self contact, or contact with the adjacent surface occurs, upon which the applied load will rise again due to crushing of the fibril. Now, when the direction of motion of the fibril tip is reversed (i.e., the probe is retracted in the experiment), the applied load will reduce as crushing of the fibril is relaxed, but then it will rise again after self contact or contact with the adjacent surfaces is eliminated and the detached surface partially readheres in a stable manner, enabling the system to follow a line equivalent to the line from C to D in Fig. 2. Finally, at a point equivalent to D in Fig. 2, dynamic reattachment will occur and the load will jump either to a point close to the upper buckling limit line or to a point on the elastic loading and unloading line in Fig. 2, then fall back to zero as the path to the origin is followed.

It is notable that we have predicted hysteresis that can lead to a history dependent behavior of the set of fibrils when they are compressed and then the compression is reversed, even though the material behavior is assumed elastic and the adhesive contact is described by a reversible constitutive law. This behavior is caused by nonlinear geometric effects introduced by the fibril buckling and unbuckling. These nonlinear geometric effects lead to the occurrence of instabilities and the resulting dynamic behavior induces dissipative processes, which are not further resolved in the presented model.

Note that if retraction of the probe is continued after the load has been reduced to zero, so that the fibrils are extended, eventually detachment under tension will occur, breaking the adhesion. This will take place due to the presence of the very small detachments we have assumed in this case, characterized by results that

have been provided by Spuskanyuk et al. [10] for the detachment of such fibrils with small edge defects in their adhesion. As a consequence, the adhesion is likely to be quite robust and the pull-off load to be relatively high. Note however, that the pull-off load will have been unaffected by the fact that the fibrils went through a process of buckling and unbuckling and that hysteresis was present in the compression cycle. This is a point we return to below.

Now consider the more complicated case of compression of a system of fibrils under load control, but where there is a very small initial detachment. The behavior is the same as under displacement control until the point marked A in Fig. 2 is reached. At this stage, the very small detachment at the end of the buckled fibril becomes fully opened and the energy release rate at its tip begins to rise above zero. If the initial detachment is small enough, this increase of the energy release rate is associated with an increasing applied load (in contrast to the examples above, where the increase of energy release rate is associated with a decreasing applied load). In that case, a small stable increase of the applied load is possible, while following a line quite close to the upper thick line in Fig. 2, until the energy release rate is finally equal to the work of adhesion. It can be shown that this critical state is unstable under load control and thus there is no stable solution other than one involving fibrillar self contact, contact of the fibril with the adjacent surfaces at its base and tip, and therefore crushing of the fibrils. This will occur with a very large jump in the motion of the fibril tips towards the fibril bases until sufficient fibril crushing has occurred to build up the equilibrium applied load to the requisite level. Further increase of the applied load will induce a very stiff behavior, involving quite small motions of the fibril tip, since such response requires further elastic crushing of the fibrils. When the applied load is thereafter reduced, the stiff response will be reversed and will continue until fibril self contact or its contact with the adjacent surfaces at its tip or base are eliminated, so that the load-displacement path has a steep slope involving little probe displacement until the load has fallen to the level close to the thick, almost horizontal line in Fig. 2 that denotes the buckling load and postbuckling response of a fibril whose tip is free to rotate. When the load is then reduced below this level, sudden unbuckling of the fibrils will occur. They will reattach to the stiff surface, and the distance between the stiff surface and the base of the fibrils will suddenly increase through a significant retraction of the probe. This returns the system to the linear elastic loading and unloading line at or near the point R in Fig. 2, and when the applied load is further reduced, the displacement of the tip will fall to zero. As before, when the fibrils are subject to tension, they will extend and finally detach by the mechanism characterized by Spuskanyuk et al. [10], controlled by the very small initial detachment under consideration. Note that the pull-off load will be unaffected by the prior buckling and unbuckling of the fibrils, the fact of hysteresis in the load cycle, and the question of whether displacement or load control was utilized.

All the models and numerical computations described so far neglect the dynamic effects that accompany instabilities associated with buckling and unbuckling of fibrils and the sudden extension or elimination of detachments on their tips. However, during such dynamic detachment extension and elimination, potential energy is released. This energy must be somehow absorbed, with kinetic energy and dissipation being the possible destinations. Consequently, inertia, viscosity and other mechanisms that absorb or dissipate energy will play an important role in the behavior of a surface patterned with fibrils that adheres to a stiff probe and is caused by compression to buckle and unbuckle. We note that both inertia and dissipative processes introduce a characteristic time into the behavior, signifying the rate at which the system can respond, given the dominance of either momentum or dissipation.

For example, if the fibrils are pulled very quickly away from the probe that is compressing them and that had caused them to buckle, full reattachment of their tips to the probe may not be possible. As a result, the adhesion of the fibril tips to the probe will not be fully redeveloped and separation of the fibril tips from its surface will be achieved easily. This situation would result in sudden pull-off of the fibrils from the probe at low force as has been observed by Paretkar et al. [9]. Thus, the pull-off force for fibrils that have been buckled in compression in this manner and then separated from the probe surface will be quite low compared to when the tips are fully adhered over their entire end, as will be the case when the fibrils never buckle, or when the retraction speed of the probe is low. Similar effects can be expected when dissipation dominates such as when the viscous component of the fibril mechanical response absorbs much energy during deformation. Other effects are possible, due to the fact that fibrils can communicate mechanically with each other through deformations of the compliant surface upon which they are patterned. For example, if the released energy is not completely absorbed or dissipated in the fibril itself, the work can be transferred to other fibrils, possibly resulting in cascades of fibril buckling and unbuckling, and tip detachment and attachment, even for fibrils compressed against spherical shapes or uneven surfaces. If some fibrils are in tension and others are in compression in such a situation, as is usually the case when a stiff, spherical probe is compressed against a flat surface patterned with fibrils, the released potential energy during dynamic detachment or attachment for those fibrils in compression that are experiencing postbuckling behavior can enhance the likelihood of pull-off for those fibrils still in tension elsewhere.

Glassmaker et al. [3] observed that the effective work of adhesion and thus the pull-off force for fibrils patterned on flat surfaces during indentation by a stiff, spherical probe differed significantly between cases where fibril buckling did and did not occur. In the case where buckling did occur, the pull-off force for the spherical probe was sometimes dramatically decreased, perhaps consistent with our argument that rate effects combined with buckling can reduce the adhesion of fibrils to the probe. However, Noderer et al. [12] report that buckling is not detrimental to adhesion if the fibrillar surface is film-terminated. A possible reason for this observation is, that the terminating film eliminates edge defects and reduces stress concentrations in the interface between fibrils and indenter. Therefore, the fibrils may not detach during buckling. In the case that the fibrils detach nevertheless, it is likely that the terminating film enhances their reattachment upon unbuckling.

Note that lateral sliding of adhered fibril tips relative to the probe may occur due to the dynamics associated with sudden detachment extension and elimination as well as because of lateral forces that can be present in the buckled configuration of a fibril. This feature would strongly influence adhesion and probably decrease the pull-off force. It is notable that load-displacement curves obtained by Sharp et al. [5] during compression by a flat indenter of platelike fibrils having a rectangular cross-section and patterned on a flat surface show a slightly positive displacement offset after a compressive load cycle. This may indicate lateral sliding of the fibrils on the probe surface, though other explanations for this phenomenon are possible (e.g., fibrils having nonuniform length). Also, in the pull-off experiments of Glassmaker et al. [3] lateral sliding may have been a source for the measured decay in adhesive performance of previously buckled fibrils. Given the fact that the longer side of the cross-section of the fibrils in these experiments is only one order of magnitude smaller than the radius of the spherical indenter, it seems possible that lateral sliding occurred during buckling due to the distortion of the fibrils caused by the curvature of the indenter. We expect that a film termination of the fibrillar surface (as examined by Noderer et al. [12]) can reduce or eliminate lateral sliding effects.

Other effects of friction are possible, such as the generation of residual stresses in a fibril near its adhered end due to its tip sliding on the probe surface to which it is adhered, with relaxation of the residual stresses being resisted by friction. Furthermore, after a fibril tip has detached during fibril buckling, the load carrying ligament of the fibril tip that is still attached to the compressing probe is subject to high stress. The resulting strain, combined with high shear stress on the remaining ligament of the fibril tip that is still attached to the stiff, compressing probe surface can result in

significant residual stress when the fibril tip is later more fully reattached to the probe surface. The strain energy associated with this residual stress, along with possible stress concentrations, can be expected to ease subsequent fibril pull-off.

Note also that we have neglected the compliance of the substrate upon which the fibrils are patterned. The elasticity of the substrate may have a strong influence on the boundary conditions at the fibril ends and therefore on the appearance of the load-displacement curves and the occurrence of the instabilities that we have described. This fact has to be kept in mind if the results presented here are compared with experimental data.

5 Conclusions

The behavior in buckling and postbuckling is analyzed for a fibril having a rectangular cross-section and that is compressed by a rigid platen to which one of its ends adheres while its other end is firmly attached to a rigid foundation. The platen is free to move sideways without constraint. The results are obtained by use of Euler–Bernoulli theory so that they are valid only for slender fibrils, and the specific case of one having an aspect ratio of 10 is studied. The initial buckling occurs at the load consistent with the buckling of a column whose ends are forbidden to rotate. Later, during postbuckling, the compressive load at one side of the adhered tip relaxes to zero and then tends to become tensile, limited by the adhesive properties of the tip. Such a situation leads to this side of the fibril tip separating from the platen, and extension of the detachment as further postbuckling displacement occurs. Eventually, the fibril has buckled so much that it makes contact with itself or with the platen and foundation and continued compression involves fibril crushing. As the material is assumed to be elastic, the buckling reverses when allowed to do so. The complex behavior involved leads to hysteresis loops in the load deflection curves, with the details depending on whether load or displacement control is invoked. Rate effects from various sources can inhibit the reversibility of the process as can deformation of the foundation caused by the buckling and unbuckling of neighboring fibrils. These effects are thought to contribute to the irreversibility of fibril adhesion upon buckling that is observed in experiments. Additionally, transfer of energy from fibrils experiencing dynamic postbuckling behavior to other fibrils being in tension may also lead to an apparent decrease in adhesive performance.

Acknowledgment

The authors wish to thank P. Neumeister for helpful discussions. They are also grateful to H. Balke for his suggestions that helped them improve the clarity of the paper.

Appendix A: Model for Postbuckling Behavior

A simplified beam model for an adhering fibril is shown in Fig. 4. The notation is defined in the figure. Furthermore, we use the abbreviation $\mathrm{d}()/\mathrm{d}z = ()'$.

Since a plane configuration of thickness h is assumed, the geometric moment of inertia I and the cross sectional area A are given by

$$I = \frac{b^3 h}{12} \qquad A = bh \tag{A1}$$

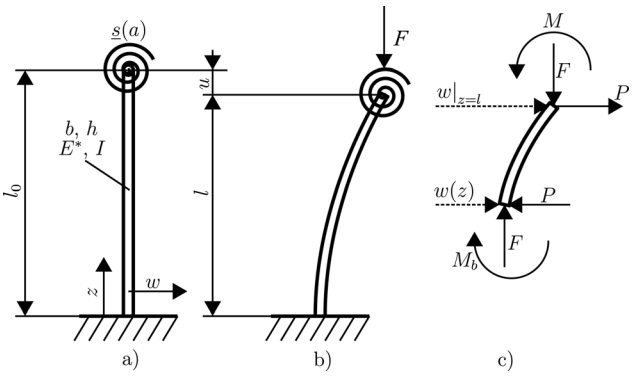

Fig. 4 (*a*) Undeformed configuration, (*b*) deformed configuration, (*c*) free body diagram

The detachment is taken into account by the compliance matrix $\underline{s}(a)$, where a is the length of the detachment on the end of the fibril. This matrix includes only the additional compliance due to the detachment because the compliance of the completely adhered configuration is already included in the beam model. The additional displacement, u_{det}, due to the detachment and the end rotation, φ_{det}, can be expressed as

$$\begin{bmatrix} u_{\mathrm{det}} \\ \varphi_{\mathrm{det}} \end{bmatrix} = \underbrace{\begin{bmatrix} s_{FF} & s_{MF} \\ s_{MF} & s_{MM} \end{bmatrix}}_{\underline{s}(a)} \begin{bmatrix} F \\ M \end{bmatrix} \tag{A2}$$

Note that the symmetry of the matrix $\underline{s}$ has been used.

The boundary conditions for the bending problem are

$$\begin{aligned} w|_{z=0} &= 0 \\ w'|_{z=0} &= 0 \\ P = 0 \quad \text{or} \quad w|_{z=l} &= 0 \end{aligned} \tag{A3}$$

where the last condition depends on the lateral boundary condition at the fibrils tip. If the lateral displacement is not constrained (configuration as in Fig. 4), the shear force P has to be zero, while in the opposite case no sidewards deflection is allowed.

Furthermore, continuity of rotations requires

$$\varphi_{\mathrm{det}} = s_{MF}F + s_{MM}M = w'|_{z=l} \tag{A4}$$

The differential equation for the problem can be derived by establishing the quasistatic balance of moments according to Fig. 4(*c*)):

$$w'' + \frac{F}{E^*I}w = \frac{F}{E^*I}|w|_{z=l} - \frac{M}{E^*I} + \frac{P}{E^*I}(l - z) \tag{A5}$$

Here the relationship $M_b = -E^*Iw''$, which connects the bending moment M_b with the approximated curvature of the beam, is used.

The solutions, which satisfy the boundary conditions (A3), are given by

$$\begin{aligned} w &= Cw_0(z, \lambda) \\ w_0 &= \begin{cases} 1 - \cos(\lambda z) & \text{if} \quad P = 0 \\ [\lambda l - \sin(\lambda l)][\cos(\lambda z) - 1] - [\cos(\lambda l) - 1][\lambda z - \sin(\lambda z)] & \text{if} \quad w|_{z=l}=0 \end{cases} \\ \lambda &= \sqrt{\frac{F}{E^*I}} \end{aligned} \tag{A6}$$

where the "shape function" w_0 is dependent on the set of boundary conditions. The constant C is connected to the end moment $M = -E^* I w''|_{z=l}$ at the fibril tip. By substituting Eqs. (A6) into (A4) we can determine C:

$$C = \frac{s_{MF} F}{w_0'|_{z=l} + s_{MM} E^* I w_0''|_{z=l}} \tag{A7}$$

This reduces the variables of the problem to F, l (or u) and a. Since one of these parameters is prescribed, two equations are required.

The first equation can be found by postulating conservation of mass. In standard Euler–Bernoulli beam theory this is equivalent to the requirement that the arc length of the beam is changed only due to axial forces. In our problem, the length is additionally changed by the extra deformations due to the detachment. This yields the equation

$$\begin{aligned}\Delta l_0 = 0 = l_0 - \underbrace{\int_0^l \sqrt{1 + (C w_0')^2}\, dz}_{\text{arc-length deformed beam}} - \underbrace{\frac{F l_0}{E^* A}}_{\text{axial compression}} - \underbrace{(s_{FF} F + s_{MF} M)}_{u_{\text{det}}} \\ \approx l_0 - l - \frac{1}{2} C^2 \int_0^1 w_0'^2 \mathrm{d}z - F\left(\frac{l_0}{E^* A} + s_{FF}\right) + s_{MF} \cdot C \cdot E^* I w_0''|_{z=l}\end{aligned} \tag{A8}$$

where Δl_0 identifies the function given by the right hand side. A Taylor-series expansion is used for the integrand in Eq. (10). A virtually identical approach was previously used by Begley and Barker [11]. The approximation is very good even for relatively large deformations. The error stays well below 1% for $w' < 0.5$. This causes no limitation on validity, since the curvature approximation with w'' is only good within 10% as long as the slope of the deflected beam stays below $w' \approx 0.3$.

The second equation represents the equilibrium condition at the detachment tip ("detachment equilibrium"). For an admissible state, the energy release rate of the system has to be equal to the work of adhesion. Expressed in terms of stress intensity factors, this gives the requirement for an increment of a

$$\begin{aligned}\Delta K = 0 &= \sqrt{\frac{E^*}{h}}\left(\sqrt{\frac{\mathrm{d}s_{MM}}{\mathrm{d}a}} M - \sqrt{\frac{\mathrm{d}s_{FF}}{\mathrm{d}a}} F\right) - \sqrt{2E^* W_{\text{ad}}} \\ &= \sqrt{\frac{E^*}{h}}\left(-\sqrt{\frac{\mathrm{d}s_{MM}}{\mathrm{d}a}} \cdot C \cdot E^* I w_0''|_{z=l} - \sqrt{\frac{\mathrm{d}s_{FF}}{\mathrm{d}a}} F\right) - \sqrt{2E^* W_{\text{ad}}}\end{aligned} \tag{A9}$$

where the first term in brackets corresponds to the stress intensity factor due to the moment M and the second term to the stress intensity factor due to the force F. Note that the stress intensity factor due to the force F is always negative, while the moment M opens the detachment. The last term is the critical stress intensity factor, which is determined from the work of adhesion by using the relationship between energy release rate and stress intensity factor Eq. (1).

We apply the normalizations and definitions

$$\begin{aligned}&z = \frac{z}{l}, \quad \bar{l} = \frac{l}{l_0}, \quad \Delta\bar{l}_0 = \frac{\Delta l_0}{l_0}, \quad \bar{a} = \frac{a}{b}, \quad \bar{b} = \frac{b}{l_0}, \quad \bar{C} = \frac{C}{l} \\ &\kappa^2 = \lambda^2 l^2 = \frac{F l^2}{E^* I} \\ &\bar{s}_{FF} = \frac{E^* A}{b} s_{FF}, \quad \bar{s}_{MF} = \frac{E^* I}{b^2} s_{MF}, \quad \bar{s}_{MM} = \frac{E^* I}{b} s_{MM} \\ &\Delta\bar{K} = \frac{\Delta K}{E^* \sqrt{b}}, \quad \bar{K}_{\text{ad}} = \sqrt{\frac{2W_{ad}}{bE^*}} \\ &\frac{\mathrm{d}(\,)}{\mathrm{d}\bar{z}} = (\dot{}\,)\end{aligned} \tag{A10}$$

Inserting the expressions for I and A into Eqs. (A9)–(A11) finally gives us the following nonlinear equations:

$$\begin{aligned}\Delta\bar{l}_0 = 0 = 1 - \bar{l} - \frac{1}{2}\bar{C}^2 \bar{l} \int_0^1 \dot{w}_0^2 \mathrm{d}\bar{z} - \frac{1}{12}\kappa^2 \frac{\bar{b}^2}{\bar{l}^2}(1 + \bar{b}\bar{s}_{FF}) \\ + \bar{s}_{MF} \frac{\bar{b}^2}{\bar{l}} \bar{C} \ddot{w}_0|_{\bar{z}=1}\end{aligned} \tag{A11}$$

$$\Delta\bar{K} = 0 = -\bar{C}\ddot{w}_0|_{\bar{z}=1} \frac{\bar{b}}{\bar{l}} \sqrt{\frac{1}{12}\frac{\mathrm{d}\bar{s}_{MM}}{\mathrm{d}\bar{a}}} - \frac{1}{12}\kappa^2 \frac{\bar{b}^2}{\bar{l}^2} \sqrt{\frac{\mathrm{d}\bar{s}_{FF}}{\mathrm{d}\bar{a}}} - \bar{K}_{\text{ad}} \tag{A12}$$

with

$$\bar{C} = \frac{\bar{b}^2}{\bar{l}} \cdot \frac{\kappa^2 \bar{s}_{MF}}{\bar{l}\ddot{w}_0|_{\bar{z}=1} + \bar{b}\ddot{w}_0|_{\bar{z}=1}\bar{s}_{MM}} \tag{A13}$$

The integral in Eq. (A11) can be found analytically given the function w_0 in Eq. (A6). Equations (A11) and (A12) are dependent on the normalized detachment length $\bar{a}$, the normalized distance $\bar{l}$ between both ends of the fibril in the deformed configuration, and the normalized force κ^2. We prescribe one of these quantities and solve numerically for the other two. For the results presented here, detachment lengths $\bar{a}$ are prescribed and we solve the equations for $\bar{l}$ and κ^2.

The stability of a solution for the case of displacement control ($\bar{l} = \text{constant}$) can be examined based on the derivative

$$\left.\frac{\mathrm{d}\Delta\bar{K}}{\mathrm{d}\bar{a}}\right|_{\bar{l}=\text{constant}} = \frac{\partial\Delta\bar{K}}{\partial\bar{a}} - \frac{\partial\Delta\bar{K}}{\partial\kappa} \cdot \frac{\dfrac{\partial\Delta\bar{l}_0}{\partial\bar{a}}}{\dfrac{\partial\Delta\bar{l}_0}{\partial\kappa}} \tag{A14}$$

The detachment equilibrium is stable if this quantity is negative und unstable if it is positive. For a vanishing derivative, higher order contributions must be examined.

In the case of load control we have to rewrite Eqs. (A11) and (A12) in terms of $\kappa_0 = \kappa/\bar{l}$ instead of κ. This is necessary, because the quantity κ depends itself on the longitudinal displacement $l_0 - l$. The derivative for the stability criterion then becomes:

$$\left.\frac{\mathrm{d}\Delta\bar{K}}{\mathrm{d}\bar{a}}\right|_{\kappa_0=\text{constant}} = \frac{\partial\Delta\bar{K}}{\partial\bar{a}} - \frac{\partial\Delta\bar{K}}{\partial\bar{l}} \cdot \frac{\dfrac{\partial\Delta\bar{l}_0}{\partial\bar{a}}}{\dfrac{\partial\Delta\bar{l}_0}{\partial\bar{l}}} \tag{A15}$$

The compliances $\bar{s}_{FF}$, $\bar{s}_{MM}$, and $\bar{s}_{MF}$ are deduced from fracture mechanics solutions for an edge cracked plate of width b. The shape functions for the stress intensity factor solutions from Tada et al. [13] are integrated and functionally fitted to get normalized compliances, which read as follows:

$$\begin{aligned}\bar{s}_{MM} &= \frac{\bar{a}^2}{(1-\bar{a})^2}\left(5.912 - 19.751\bar{a} + 41.94\bar{a}^2 - 55.509\bar{a}^3 \right. \\ &\quad \left. + 39.497\bar{a}^4 - 11.429\bar{a}^5\right) \\ \bar{s}_{FF} &= \frac{\bar{a}^2}{(1-\bar{a})^2}\left(1.975 - 3.178\bar{a} + 7.391\bar{a}^2 - 7.524\bar{a}^3 \right. \\ &\quad \left. + 4.059\bar{a}^4 - 0.746\bar{a}^5\right) \\ \bar{s}_{MF} &= \frac{\bar{a}^2}{(1-\bar{a})^2}\left(-0.987 + 2.461\bar{a} - 5.105\bar{a}^2 + 6.497\bar{a}^3 \right. \\ &\quad \left. - 4.449\bar{a}^4 + 1.253\bar{a}^5\right)\end{aligned} \tag{A16}$$

Great care was taken to represent the correct asymptotic behavior for $\bar{a} \to 1$. This is necessary to ensure a robust numerical solution of the nonlinear equations for deep detachments, because of the divergence of the compliances. Comparison of the compliance based stress intensity factor solutions with the results from [13] yields deviations less than 0.5% for all detachment lengths. Since the formulae in Ref. [13] are claimed to have 0.5% accuracy, the overall accuracy of the compliance based stress intensity factors should be better than 1%.

The procedure presented is valid only for an open detachment. For a completely attached fibril with $\bar{a} = 0$ the compliances due to the detachment are zero, and this state controls the initial buckling. In this case, we get from Eq. (A4) the boundary condition

$$\dot{w}_0|_{\bar{z}=1} = 0 \tag{A17}$$

The solution for initial buckling consistent with this boundary condition is $\kappa^2 = \kappa^2_{\text{buckling}} = \pi^2$ for the case without lateral constraint and $\kappa^2 = \kappa^2_{\text{buckling}} = 4\pi^2$ for completely clamped boundary conditions. With this in hand, we can prescribe $\bar{l}$ and get $\bar{C}^2$ from Eq. (A11):

$$\bar{C}^2 = \frac{\dfrac{2}{\bar{l}}\left(1 - \bar{l} - \dfrac{1}{12}\kappa^2_{\text{buckling}}\dfrac{\bar{b}^2}{\bar{l}^2}\right)}{\displaystyle\int_0^1 (\dot{w}_0)^2 \mathrm{d}\bar{z}} \tag{A18}$$

The quadratic form arises from the undetermined buckling direction. It is obvious, that this equation has only a real root if the condition

$$12(1 - \bar{l})\frac{\bar{l}^2}{\bar{b}^2} \geq \kappa^2_{\text{buckling}} \tag{A19}$$

is met. This condition governs the existence of buckling. If the displacements are too small ($\bar{l}$ too close to 1), the criterion is not fulfilled and consequently a buckled shape is not possible. Then the only valid solution is the compression of a straight bar. In this case force and axial displacement are simply connected through

$$\kappa^2 = 12(1 - \bar{l})\frac{\bar{l}^2}{\bar{b}^2} \tag{A20}$$

Note that κ^2 depends itself on the displacement. Thus, it is advantageous for the interpretation of the results, to rewrite Eq. (A20) in terms of $\kappa_0 = \kappa/\bar{l}$:

$$\kappa_0^2 = 12(1 - \bar{l})\frac{1}{\bar{b}^2} \tag{A21}$$

This is the expected linear elastic relationship between force and displacement for a straight bar.

Appendix B: Finite Element Model

To obtain numerical results, a two dimensional plane strain finite element model of a fibril was developed. The main features are schematically depicted in Fig. 5(*a*).

The mesh is built from 8-noded reduced integration elements. At the adhering surface the elements have uniform size. The transition between the fine mesh of this region and the coarser mesh of the remaining model is realized with multi point constraints.

The nonadhering end of the fibril at the top of the model in Fig. 5 is constrained to move as dictated by a rigid body. This rigid body is not allowed to rotate.

The adhering surface at the bottom of the model is assumed to be frictionless. Thus, nodes on the attached ligament are not allowed to move in the x_2-direction, while movement in the x_1-direction is unconstrained.

Axial compression is prescribed by the displacement u_2 of the rigid body at the top, while its lateral displacement u_1 is set to zero.

The propagation of the detachment is implemented by eliminating the displacement boundary condition for the nodes on the adhering end of the fibril. During closure of the detachment, these displacement boundary conditions are reactivated.

The simulation is conducted with the commercial finite element software ABAQUS.

In a first step, buckling is initiated by increasing the axial displacement $-u_2$ slightly above its critical value. A small rotation of the rigid body is used to introduce the necessary imperfection inducing buckling. After buckling is initiated, this rotation is removed in a second step.

Thereafter, the axial displacement is incremented in small steps. After each step the behavior of the detachment is evaluated. For this purpose two separate finite element calculations are conducted (except in the cases of a completely adhered fibril and a completely detached fibril). The procedure is schematically shown in Fig. 5(*b*). The initial state for both calculations is the result from the previous displacement increment step, for which the strain energy W and detachment length a are known. Note, that the detachment length is always measured in the undeformed configuration. During the first calculation, the detachment is extended by one element. This increases the detachment length by the

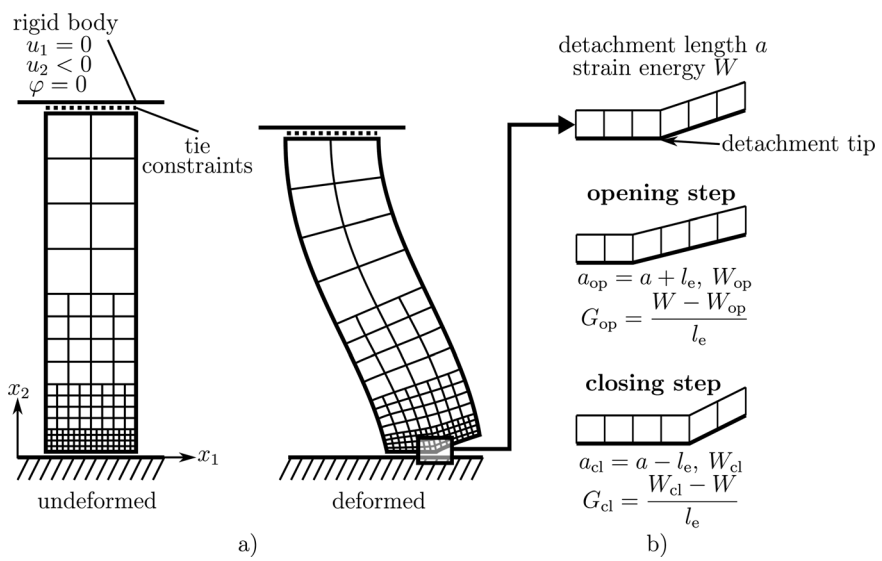

Fig. 5 (*a*) Finite element model; (*b*) evaluation of detachment behavior

element width l_e to the new detachment length a_{op}. The strain energy for the new state W_{op} is then used to determine the energy release rate G_{op}. The detachment closure calculation is treated analogously. In the case of zero detachment length only opening of the detachment is simulated and for a completely detached fibril only detachment closure is computed.

Since no contact is modeled, all computed energy release rates are positive. To identify overclosure of the detachment the displacement of the first nonmidside node on the detached surface behind the detachment tip is examined. If this node penetrates the line $x_2 = 0$, the energy release rate is set to an arbitrary negative value to indicate overclosure of the detachment.

Finally, the computed energy release rates are compared with the given work of adhesion $W_{ad}(a)$, which can be dependent of the detachment length a, e.g., the adhesion energy is zero for the initial detachment but is greater than zero elsewhere. In the cases of $G_{op} < W_{ad}(a_{op})$, $G_{cl} < W_{ad}(a_{cl})$ or $G_{op} = W_{ad}(a_{op})$ or $G_{cl} = W_{ad}(a_{cl})$ the detachment length remains unchanged and the next axial displacement increment is applied. For $G_{op} > W_{ad}(a_{op})$, $G_{cl} > W_{ad}(a_{cl})$ the detachment is propagated element by element until the energy release rate drops below W_{ad}. In order to avoid oscillations in detachment length in the course of the simulation, the last detachment propagation increment is always undone before the next displacement step. Closure of the detachment in the case of $G_{op} < W_{ad}(a_{op})$, $G_{cl} < W_{ad}(a_{cl})$ is treated in the same way. For zero detachment length $G_{cl} > W_{ad}$ is assumed and for a completely detached fibril $G_{op} < W_{ad}$ is taken. Note that it is not possible to determine the direction of detachment propagation for the case $G_{op} > W_{ad}(a_{op})$, $G_{cl} < W_{ad}(a_{cl})$ with a static analysis. However, this situation was not encountered.

Initially, the adhering tip of the fibril is completely attached. To introduce an initial detachment of length a_{init}, the work of adhesion is defined to be zero on the corresponding surface. On the remaining surface the work of adhesion is taken to be greater than zero and uniform.

With the procedure described sudden detachment and attachment due to the occurrence of an unstable detachment equilibrium can be taken into account during displacement controlled hysteresis. To obtain accurate results it is necessary to choose the displacement and detachment length increments sufficiently small. The latter requires an adequate mesh refinement.

The calculations are done for a linear elastic isotropic material even though the effect of nonlinear geometry is included to allow for buckling. The Poisson's ratio is set to 0.45.

References

[1] Arzt, E., Gorb, S., and Spolenak, R., 2003, "From Micro to Nano Contacts in Biological Attachment Devices," Proc. Natl. Acad. Sci. U.S.A., **100**, pp. 10603–10606.

[2] Boesel, L. F., Greiner, C., Arzt, E., and del Campo, A., 2010, "Gecko-Inspired Surfaces: A Path to Strong and Reversible Dry Adhesives," Adv. Mater., **22**, pp. 2125–2137.

[3] Glassmaker, N. J., Jagota, A., Hui, C.-Y., and Kim, J., 2004, "Design of Biomimetic Fibrillar Interfaces: 1. Making Contact," J. R. Soc., Interface, **1**, pp. 23–33.

[4] Hui, C.-Y., Jagota, A., Shen, L., Rajan, A., Glassmaker, N., and Tang, T., 2007, "Design of Bio-Inspired Fibrillar Interfaces for Contact and Adhesion—Theory and Experiments," J. Adhes. Sci. Technol., **21**, pp. 1259–1280.

[5] Sharp, K. G., Blackman, G. S., Glassmaker, N. J., Jagota, A., and Hui, C.-Y., 2004, "Effect of Stamp Deformation on the Quality of Microcontact Printing: Theory and Experiment," Langmuir, **20**, pp. 6430–6438.

[6] Gao, H., Wang, X., Yao, H., Gorb, S., and Arzt, E., 2005, "Mechanics of Hierarchical Adhesion Structures of Geckos," Mech. Mater., **37**, pp. 275–285.

[7] Yao, H. G. H., 2004, "Shape Insensitive Optimal Adhesion of Nanoscale Fibrillar Structures," Proc. Natl. Acad. Sci., **101**, pp. 7851–7856.

[8] Gao, H. Y. H., 2006, "Mechanics of Robust and Releasable Adhesion in Biology: Bottom-Up Designed Hierarchical Structures of Gecko," J. Mech. Phys. Solids, **54**, pp. 1120–1146.

[9] Paretkar, D., Kamperman, M., Schneider, A. S., Martina, D., Creton, C., and Arzt, E., 2011, "Bioinspired Pressure Actuated Adhesive System," Mater. Sci. Eng. C, **31**, pp. 1152–1159.

[10] Spuskanyuk, A. V., McMeeking, R. M., Deshpande, V. S., and Arzt, E., 2008, "The Effect of Shape on the Adhesion of Fibrillar Surfaces," Acta Biomater., **4**, pp. 1669–1676.

[11] Begley, M. R., and Barker, N. S., 2007, "Analysis and Design of Kinked (Bent) Beam Sensors," J. Micromech. Microeng., **17**, pp. 350–357.

[12] Noderer, W., Shen, L., Vajpayee, S., Glassmaker, N., Jagota, A., and Hui, C.-Y., 2007, "Enhanced Adhesion and Compliance of Film-Terminated Fibrillar Surfaces," Proc. R. Soc. London, Ser. A, **463**, pp. 2631–2654.

[13] Tada, H., Paris, P. C., and Irwin, G. R., 1985, *The Stress Analysis Handbook*, 2nd ed., Paris Productions Incorporated, St. Louis, MO.